**Titel/Title:** Atomistic Modeling of the Formation of a Thermoset/Thermoplastic Interphase during Co-Curing

**Autor*innen/Author(s):** Magdalena Laurien, Baris Demir, Holger Büttemeyer, Axel S. Herrmann, Tiffany R. Walsh, and Lucio Colombi Ciacchi

Veröffentlichungsversion/Published version: Postprint

Publikationsform/Type of publication: Artikel/Aufsatz

**Empfohlene Zitierung/Recommended citation:**

Magdalena Laurien, Baris Demir, Holger Büttemeyer, Axel S. Herrmann, Tiffany R. Walsh, and Lucio Colombi Ciacchi. Atomistic Modeling of the Formation of a Thermoset/Thermoplastic Interphase during Co-Curing. Macromolecules 2018 51 (11), 3983-3993 DOI: 10.1021/acs.macromol.8b00736

Verfügbar unter/Available at:
(wenn vorhanden, bitte den DOI angeben/please provide the DOI if available)

10.1021/acs.macromol.8b00736

# Atomistic Modelling of the Formation of a Thermoset/Thermoplastic Interphase during Co-Curing

*Magdalena Laurien[1,2], Baris Demir[3], Holger Büttemeyer[4], Axel S. Herrmann[4], Tiffany R. Walsh[3], Lucio Colombi Ciacchi[1,]**

[1]Hybrid Materials Interfaces Group, University of Bremen, Faculty of Production Engineering, Bremen Center for Computational Materials Science, Center for Environmental Research and Sustainable Technology (UFT), and MAPEX Center for Materials and Processes, 28359 Bremen, Germany.

[2]Department of Materials Science and Engineering, McMaster University, Hamilton ON L8S 4L8, Canada

[3]Institute for Frontier Materials, Deakin University, Geelong, Victoria 3216, Australia

[4]Faserinstitut Bremen, and University of Bremen, Faculty of Production Engineering, 28359 Bremen, Germany

***Corresponding author. E-Mail: colombi@hmi.uni-bremen.de. Tel. +49 421 21864570.**

ABSTRACT: Co-curing of a thermoset epoxy matrix in contact with thermoplastic foils is an essential step in damage-free joining of polymers or polymer-based composites. We present results of all-atom molecular dynamics simulations that shed light into the resulting hybrid interface. Using polyvinylidene difluoride (PVDF) and a multicomponent epoxy resin as model systems, we have developed a computational co-curing protocol that ensures both adequate structural representation and mobility of the PVDF chains and a realistic cross-linking conversion and topology of the epoxy resin. As a result, we reveal that mutually entangled loops of thermoplastic chains and resin strands form across the interface within the extended interphase region separating the two polymers. In tensile stress simulations we find that these loops contribute to a surprisingly large interfacial strength. In the absence of extrinsic defects, failures nucleate at the PVDF side of the interphase and propagate *via* a chain-pullout mechanism characteristic of semi-interpenetrating polymer networks involving thermoplastic materials.

## 1. INTRODUCTION

The ongoing effort to design novel light-weight materials brings forth entirely new material concepts, which consequently require innovative joining techniques. A prominent example is the use of carbon or other fiber-reinforced plastics (FRP) as a light-weight alternative to aluminum alloys for structural components in the aerospace sector[1]. Joining FRP with conventional riveting entails inevitable weakening of the composite structure as a consequence of cutting the reinforcing fibers across holes drilled to accommodate the rivets[2,3]. In recent years, thermoset welding, enabled by a re-meltable thermoplastic surface layer, has been developed as an innovative solution for FRP-joining that guarantees integrity of the fiber architecture[3,4].

The two-step joining procedure involves first the co-curing of a thermosetting (TS) FRP matrix with a thermoplastic (TP) foil attached to its surface. In the subsequent welding step, the TP

surfaces of two components are heated, which causes the polymer chains to soften and entangle across the surfaces, thus forming a joint. Crucial to the stability of this joint is not only a successful thermoplastic welding, but also strong adhesion of the hybrid TS/TP interface, which forms during co-curing.

In this work we focus on the molecular-scale details of such a TS/TP hybrid interface, using all-atom molecular dynamics simulations. Our aim is to provide a realistic model for the interphase region between a typical TP polymer (polyvinylidene difluoride, PVDF) and a typical multicomponent TS epoxy resin (*vide infra*). As the TS matrix and the TP layer are dissimilar in reactivity, chain size and density, it is not obvious that the interactions within the TP/TS interphase will be as strong and reliable as per the strict regulations with which aerospace components must comply[3]. Remarkably, the adhesive strength of co-cured and welded TS/TP FRP components has been found to be competitive with commercial adhesive solutions[5]. However, the molecular mechanisms governing the adhesive strength at the interphase are very poorly understood. In particular, it remains to be explored whether only physical (non-covalent) interactions between the hybrid components occur, or if instead, and under which conditions, covalent bonds may form as a result of the epoxy resin chemically reacting with the TP chains.

To date, neither the exact extent of miscibility of the components, nor the molecular topology (<- p. 3983)
of hybrid TS/TP interfaces is known. Such details are challenging to resolve *via* experimental approaches alone, which motivates the use of all-atom molecular simulation techniques in the present work. In previous simulations reported by Dumont et al.[6], smaller epoxy resin molecules were found to readily diffuse into a melt of TP oligomers (polyethersulfone and phenoxy). However, neither the effect of TS chains longer than five or six repeat units, nor the effect of epoxide-amine cross-linking reactions on the interphase formation has been investigated to date.

Here we consider both the dynamics of longer PVDF chains, of the order of 100 repeat units, and the evolution of cross-linking within the epoxy matrix, and develop an effective computational co-curing protocol to produce small-scale hybrid TS/PS interfacial models. In doing so, we explore the possible formation of a semi-interpenetrating polymer network (semi-IPN) in the interphase region, capable of capturing entanglements between the two components in a strong and stable joint. Using all-atom techniques bears the obvious disadvantage of addressing only a very small region of the interface, which extends, in the engineering reality, over many microns (Figure 1, left and center). However, this is the only technique that can provide atomistic details of the intermolecular and intramolecular interactions. The structural models produced by our work can serve as a basis for future studies addressing the possible formation of covalent bonds across the TP/TS interface (Fig 1, right).

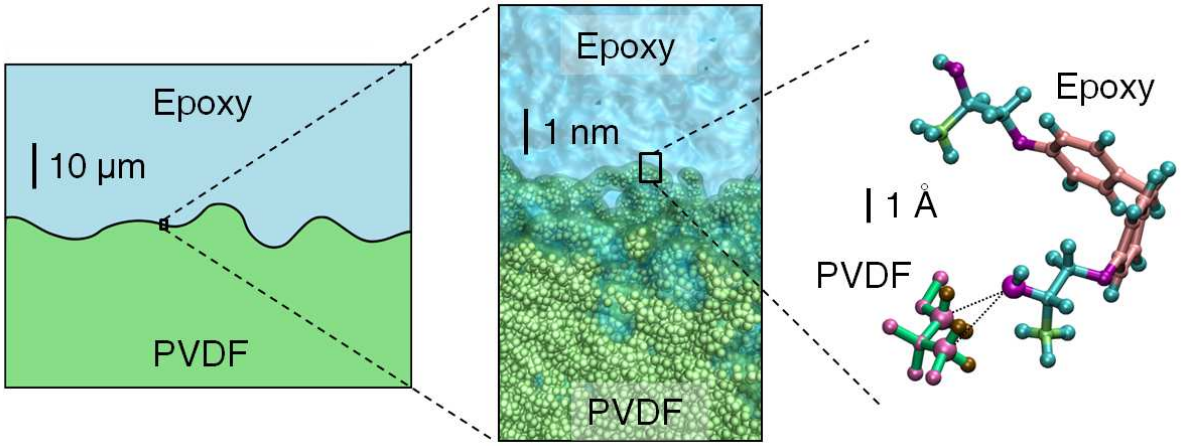


**Figure 1.** Schematic representation of a hybrid interface between an epoxy resin and a thermoplastic polymer (PVDF) at a microscopic scale (left), the nanoscopic scale accessible to all-atom molecular dynamics simulations (center), and the atomic scale with details of the atom-atom interactions (right).

## 2. METHODOLOGY

**2.1. Computational details.** All molecular dynamics (MD) simulations were carried out using the LAMMPS (lammps.sandia.gov) simulation software package[7]. The inter-atomic forces were calculated using the DREIDING[8] force field. Newton's equations of motion were time-integrated using the velocity-Verlet algorithm with a time step of 1 fs. The Nosé[9]-Hoover[10,11] thermostat and barostat were used for temperature and pressure control, respectively. Periodic boundary conditions were implemented in all directions (unless otherwise stated). The long-range electrostatic interactions were evaluated using the PPPM Ewald summation method[12]. The neighboring list cutoffs were set to 12 Å. Tail corrections were applied to compute the total energy and pressure. Partial atomic charges were calculated using the charge equilibration method (QEq) proposed by Rappe and Goddard[13], as implemented by Demir and Walsh[14]. This requires averaging of charges belonging to symmetry-equivalent atomic sites, which are part of the same unique atom environment within each molecular structure. Non-bonded interactions were calculated within 3D periodic boundaries with a Buckingham potential. All of the parameters used in this study are summarized in the Supplementary Information, Table S1 and Figures S1-S3.

(<- p. 3984)

**2.2. Thermoplastic polymer model.** As a model of the thermoplastic polymer we used linear chains of polyvinylidene difluoride (PVDF) (Figure 2b). The input structure for the bulk PVDF was created using the Polymer Modeler tool[15], randomly placing 136 chains, each consisting of 125 repeat units, in a cubic simulation cell with dimension of 15 nm. The initial packing density was deliberately set to a low value of 0.5 g/cm$^3$, and the simulation cell size was then reduced until the experimental density of 1.78 g/cm$^3$ was reached. This was realized by rescaling the atomic coordinates within the periodic simulation cell during a simulation run in the isothermal-

isobaric (*NpT*) ensemble using the LAMMPS *deform* command. A 21-step relaxation procedure was employed for an enhanced equilibration as described by Abbot et al.[16] (based on procedures published by Hofmann[17] and Larsen et al.[18]), implementing a maximum temperature of 1000 K and a maximum pressure of $5 \cdot 10^4$ bar, and targeting the final values of 500 K and 1 bar in the final step. As pointed out in the original literature[16-18], the use of a very high simulation temperature allows for complete relaxation of the degrees of freedom internal to the individual polymer chains, in particular allowing for easy rotations of the torsional angles within the connected monomers. At the same time, a high simulation pressure is required to achieve further densification of the structure created at low density, and to remove any voids that might have remained after initial compacting. This guarantees that a correct and uniform density is obtained at the end of the 21-step equilibration. The whole relaxation protocol was carried out over the simulation times of either 1.56 ns or 15.6 ns (depending on the relaxation schedule, as detailed herein), leading to a sufficiently well equilibrated PVDF melt, as represented in Figure S5 of the Supplementary Information.

**2.3 Epoxy relaxation and cross-linking.** The thermoset polymer was modelled as a mixture comprising the diglycidyl ether of bisphenol F (BIS), tetraglycidyl diaminodiphenyl methane (TGD), and triglycidyl-p-aminophenol (TRI) as epoxide monomers, and diaminodiphenyl sulphone (known also as dapsone, DDS) as the curing agent (Figure 2). A total of 3738 molecules in the approximate ratio BIS:TGD:TRI:DDS = 8:5:4:8 were used to model the liquid bulk material before cross-linking. The single molecules were built and geometry optimized using Avogadro[19] and randomly placed in a periodically repeated simulation cell with initial dimensions of 30x30x15 $nm^3$ using the Packmol[20] software package. The simulation cell size was reduced to 10x10x15 $nm^3$ (a density of 1.24 $g/cm^3$) using the LAMMPS *deform* command. The

liquid mixture was equilibrated using the same 21-step procedure used for PVDF, at the end of which the molecules were uniformly distributed in the simulation cell (see S.I., Figure S6).

Starting from the liquid epoxy/diamino mixture, a cross-linked thermoset resin was obtained via use of a slight modification of the original simulation protocol developed by Demir and Walsh[14]. This procedure allows for the formation of chemical bonds between the reactive nitrogen sites of the amino groups of the curing agent and the reactive carbon sites of the epoxy rings during a classical MD simulation run. In the simulated system, the epoxide monomers were modeled already in their 'activated' form, with terminal OH and methyl groups instead of epoxy rings (as represented in Figure S2). The cross-linking protocol is summarized in the scheme of Figure 3, and the corresponding reaction in Figure 2c.

Covalent cross-link bonds between the reactive atomic sites were created on the basis of a distance-cutoff criterion with probability of 100%, distinguishing between primary bonds formed by free terminal -$NH_2$ groups, and secondary bonds formed by -NH- groups of a pre-linked chain. Initial cutoff distances of 3.5 Å and 4.5 Å were chosen for the primary and secondary bonds, respectively. We found that choosing the same cutoff for both bond types led to a strong discrimination against the formation of secondary bonds, likely due to steric hindrances. Both cutoff values were increased by 0.5 Å each after ten cross-linking attempts, in order to compensate for the increasing stiffness and reduced mobility of the cross-linked network.

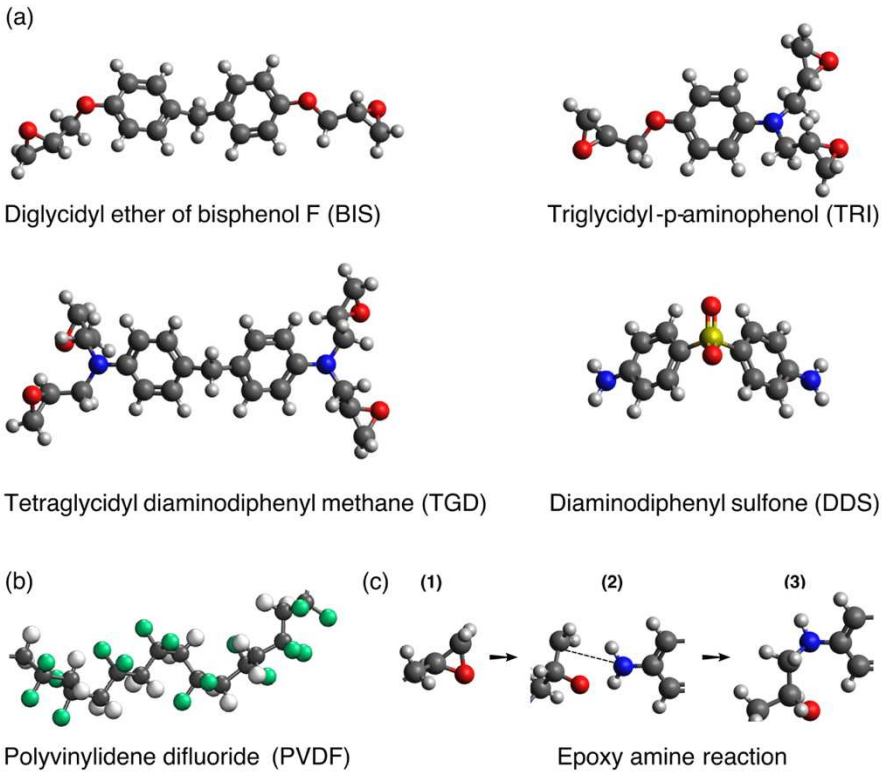


**Figure 2.** Ball-and-stick representations of all simulated molecules. Oxygen: red, carbon: grey, hydrogen: white, nitrogen: blue, fluorine: green, sulfur: yellow.

Each cross-linking cycle consisted of (1) a bond formation step; (2) a topology and charge update step; and (3) a stepwise bond equilibration step. The three steps were performed separately for primary and secondary bonds, in this order.

In the first step, all distances between the reactive atomic sites are computed. For all distances (<- p. 3985) that are smaller than the set cutoff, a covalent cross-link bond is created using the LAMMPS *bond create* function. In the second step, the reacted atoms are assigned new atom types, angles, dihedrals and charges. The excess hydrogen atoms of the amine groups (present because of the use of already activated epoxy molecules) are deleted. The partial charges of the atoms involved in the new bonds are updated to new QEq values calculated for the new topology, under the constraint of charge neutrality of the whole system[14]. In the present implementation, the topology

and charge updates are conducted on the fly within the LAMMPS code, which greatly reduces time-consuming out-of-code processing. As a technical note, we point out that LAMMPS allows for the specification of only one dihedral type when forming a new bond, whereas the newly-formed cross-linked C-N bond is involved in $sp^3$-$sp^3$ as well as $sp^2$-$sp^3$ dihedrals. However, we have found that use of $sp^3$-$sp^3$ dihedral parameters is perfectly adequate for our purposes.

In the third step, the bond-equilibration stage, the equilibrium bond distance of all newly created bonds is reduced stepwise from the cutoff value to the bond equilibrium length of the DREIDING force field, while at the same time the bond force constant is stepwise increased, starting from one tenth of the DREIDING value, up to its equilibrium value. This prevents large and sudden fluctuations of the mechanical stress in the simulation cell after the bond-creation step, which may lead to instabilities in the MD integration. Typically, the bond parameters are varied linearly in 10 steps of *NVT* simulations, each lasting 10 ps. After reaching the correct DREIDING values, an *NpT* run of 20 ps at 1 bar and 500 K is carried out to relax the stress. We found that this sequence of steps ensures the simulation stability more reliably than alternative approaches, such as those based on *NpT* runs while the bond parameters are varied.

At the conclusion of the 10 bond creation cycles (primary and secondary bonds), an *NpT* simulation lasting 50 ps was performed at 1 bar and 500 K. The bond-distance cutoff values were increased by 0.5 Å, as mentioned above, and the protocol was repeated until the number of cross-linked bonds reached saturation. In our case, saturation values of about 95% (considering both primary and secondary bonds) were obtained (as detailed in Results).

**2.4. Estimation of thermo-mechanical properties**. The bulk polymer matrices were characterized *via* calculation of the glass transition temperature, $T_g$ and the elastic Young's modulus, $E$ following the procedure of Demir and Walsh[14]. $T_g$ was obtained as the intersection

point of two linear regressions fitting the variation of density as a function of temperature. To accomplish this, the bulk systems were cooled down in a stepwise manner from the equilibration temperature of 500 K to a temperature (typically, 70 K) far below the experimentally known value of $T_g$, in steps of 10 K. At each temperature step, the system was equilibrated in the *NpT* ensemble for 0.5 ns and the density was computed as the average value obtained over the whole step. The linear fits were performed over temperature ranges of 150 K well above and below the change of slope in the obtained density-temperature curves.

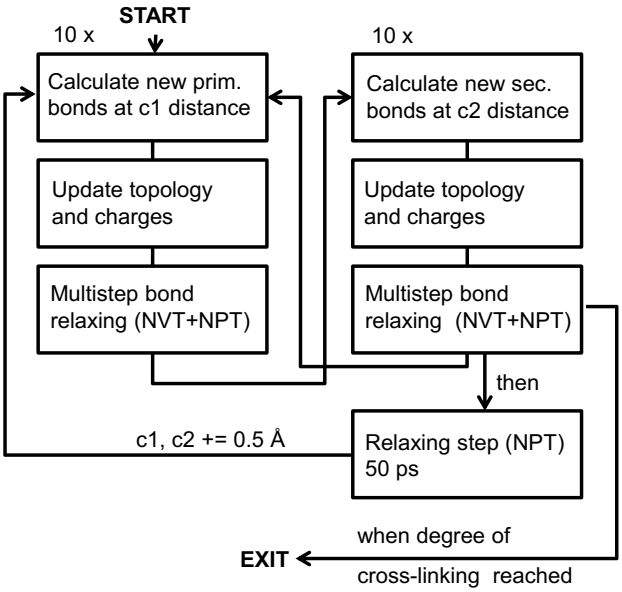


**Figure 3.** Flow chart summarizing the cross-linking algorithm. Primary and secondary cross-links are formed separately. The steps of bond-creation, topology and charge update and multistep relaxation are repeated 10 times in each cycle. After that follows a short relaxation in the NPT ensemble and the procedure is repeated until saturation of the cross-linking conversion.

The Young's moduli of the bulk systems were obtained in simulated tensile tests performed as non-equilibrium MD runs at 300 K. Strain was applied to the simulation cell with the LAMMPS *deform* command at the constant strain rates of $5 \cdot 10^{6}$, $5 \cdot 10^{7}$, and $5 \cdot 10^{8}$ $s^{-1}$ along the $z$ direction

(using the LAMMPS *erate* command), while remapping the velocities of the atoms in the same direction (using the LAMMPS *remap* command). The simulation cell was allowed to relax in the *x* and *y* directions by application of a non-uniform barostat. The components of the total stress vector were calculated from the sum of the components of the atomic force vectors divided by the initial area of the cell in the *xy* plane (engineering stress). The so-obtained stress-strain curves were linearly fitted in the region of strain up to 2%.

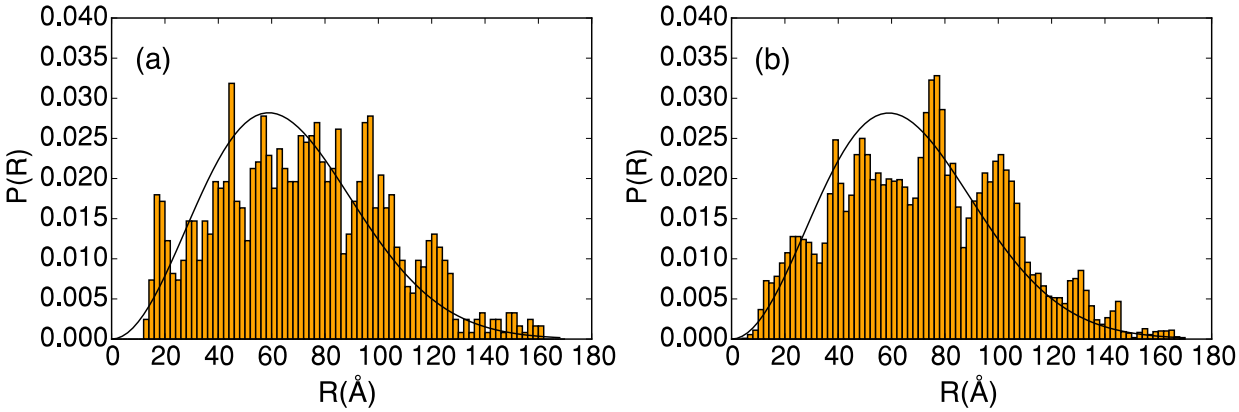


**Figure 4.** Average distribution, P (R) of the end-to-end distance R for step 1 (a), and for step 21 (b) of the 21-step equilibration procedure (1.56 ns). The black curves show the distributions predicted by the ideal freely-joined-chain model.

## 3. RESULTS

The reliable prediction of atomistic structural details at hybrid thermoplastic/thermoset interfaces during co-curing requires objective consideration of whether the model system is adequate for this purpose. In particular, it should be ensured that the thermoplastic chains are sufficiently long to form an extended interphase region, and that the mobility of all molecules (*i.e.* due to diffusion) is balanced against the rate of simulated cross-linking in the resin (conversion). These two aspects are inherently incompatible, since modelling polymer chains close to their experimental lengths would result in exceedingly large system sizes, which would

not allow us to perform MD simulations of sufficiently duration to capture adequate diffusion. For this reason, the chain lengths are chosen so that correct prediction of experimental thermo-mechanical polymer properties can be achieved within the simulation times accessible to all-atom MD simulation. This approach could be viewed as a sort of accelerated scheme, whose individual components (characteristic lengths on one side, characteristic rates on the other side) are far from the physical reality in their right, but together deliver an acceptable and physically-reasonable behavior of the experimental system. As a drawback, a quantitative assessment of the kinetics of the simulated processes is not possible, since neither the true cross-linking rate nor the true inter-diffusion coefficients are considered in the simulations. This approach is first tested for
(<- p. 3986)
the isolated thermoplastic and thermoset components before addressing the formation of a hybrid interface.

**3.1 Bulk components.** The PVDF system built with Polymer Modeler yields chains that are predominantly in the $\alpha$ configuration, with an alternating trans-gauche arrangement of the $CF_2$ moieties along the chain (Figure 2b). The structures produced by the packing algorithm (S.I., Figure S5) and relaxed *via* the 21-step protocol proposed by Abbott et al.[16] can be characterized by the histogram distribution, *P (R),* of the end-to-end length $R$, as reported in Figure 4a. This histogram can be compared to the end-to-end distance distribution of ideal freely-joined chains for the same mean $R^2$-value[21]

$$P_{3D}(R,N)4\pi R^2 dR = \left[\frac{3}{2\pi\, N\, b^2}\right]^{3/2} exp\left[-\frac{3R^2}{2N\, b^2}\right] 4\pi\, R^2 dR$$

where $P_{3D}(R,N)$ is the probability for the length of the end-to-end vector $\vec{R}$ to be within a spherical shell ranging from $R$ to $R + dR$, $N$ is the number of freely joined segments, and $b$ is their length (the Kuhn length). Here, the fit is performed with the constraint that $N{\cdot}b$ be equal to

the length of a completely outstretched chain, $R_{max}$. The latter can be computed for our chain model given the equilibrium length of the C-C bonds, $l$ = 1.53 Å, the equilibrium C-C-C angle, θ = 109.47°, and the number of bonds in each chain, $n$ = 249 (corresponding to 125 monomers):

$$Nb = R_{max} = nl\cos(\theta/2)$$

Furthermore, the average square end-to-end distance $\langle R^2 \rangle$ resulting from the fit can be employed to compute the Flory's characteristic ratio

$$C_\infty = \langle R^2 \rangle / (n\, l^2)$$

The values are summarized in Table 1 for the bulk PVDF structures directly produced by Polymer Modeler and after 21-step equilibration, both using the short-time protocol of Abbott et al.[16] (1.56 ns in total), and a longer relaxation time (15.6 ns).

**Table 1.** Properties of the PVDF chain models at 500 K before (Step 1) and after (Step 21) short (1.56 ns) and long (15.6 ns) relaxation.

| | Step 1 | Step 21 | Step 21 (15.6 ns) |
|---|---|---|---|
| $\langle R^2 \rangle$ (Å$^2$) | 5201 | 5213 | 5566 |
| $b$ (Å) | 16.72 | 16.76 | 17.89 |
| # $N$ | 18.60 | 18.56 | 17.39 |
| $C_\infty$ | 8.92 | 8.94 | 9.55 |

From the histogram in Figure 4 and the estimated structural properties in Table 1 it can be observed that the as-produced structure before relaxation already presents an acceptable distribution of end-to-end lengths, characterized by a Kuhn length ($b$) of 1.7 nm, which is in the typical range expected for linear substituted hydrocarbon chains, and a Flory's ratio of 8.9,

which is in excellent agreement with an available experimental estimate (8.9 ± 2)[22]. As mentioned in the Methods section, the application of the 21-step relaxation leads to equilibration of the intra-chain degrees of freedom (due to the high applied temperature), and to a better compaction of the chains toward their equilibrium bulk density (due to the high applied pressures). In particular, the evolution of the density during the relaxation is reported in Figure S4. In fact, only negligible variations of the properties are obtained after the short 21-step relaxation, and slight overall increases of the average end-to-end distances, Kuhn length and Flory's ratio are obtained after longer relaxation.

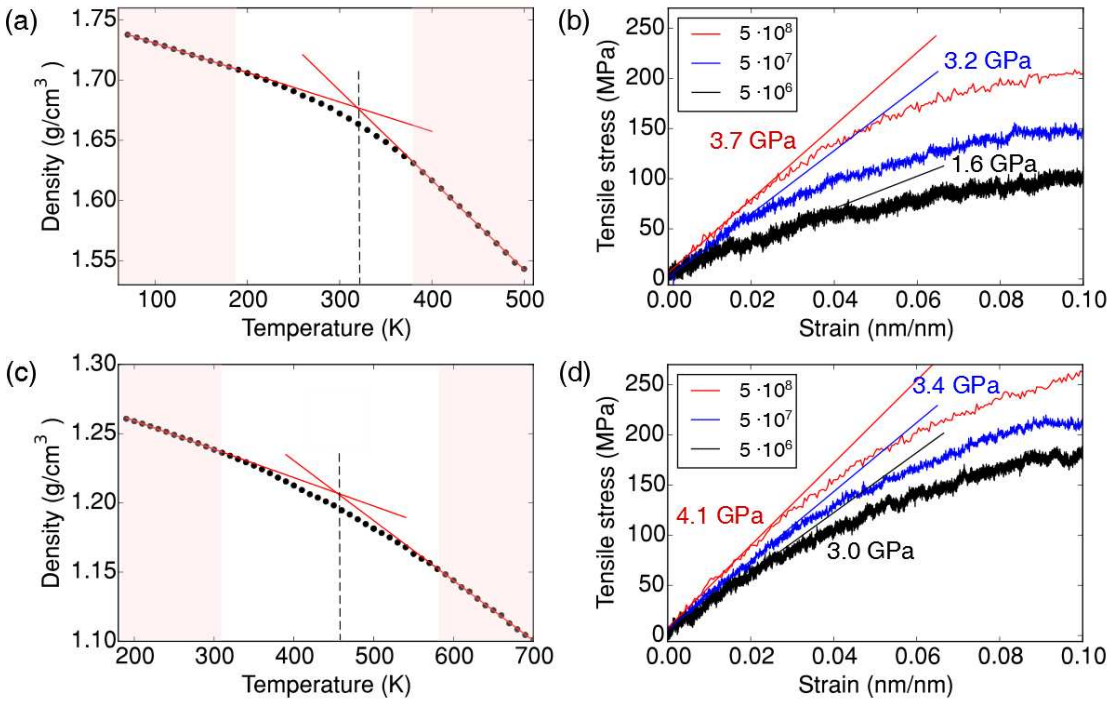


**Figure 5.** Density as a function of temperature (a,c) and tensile stress-strain curves (b,d) for PVDF (a,b) and epoxy (c,d). The glass transition temperature is estimated as the intersection of the linear fits (fitted regions shaded) of the lower and higher temperature areas (red lines in a,c).

which is in excellent agreement with an available experimental estimate (8.9 ± 2)[22]. As mentioned in the Methods section, the application of the 21-step relaxation leads to equilibration of the intra-chain degrees of freedom (due to the high applied temperature), and to a better compaction of the chains toward their equilibrium bulk density (due to the high applied pressures). In particular, the evolution of the density during the relaxation is reported in Figure S4. In fact, only negligible variations of the properties are obtained after the short 21-step relaxation, and slight overall increases of the average end-to-end distances, Kuhn length and Flory's ratio are obtained after longer relaxation.

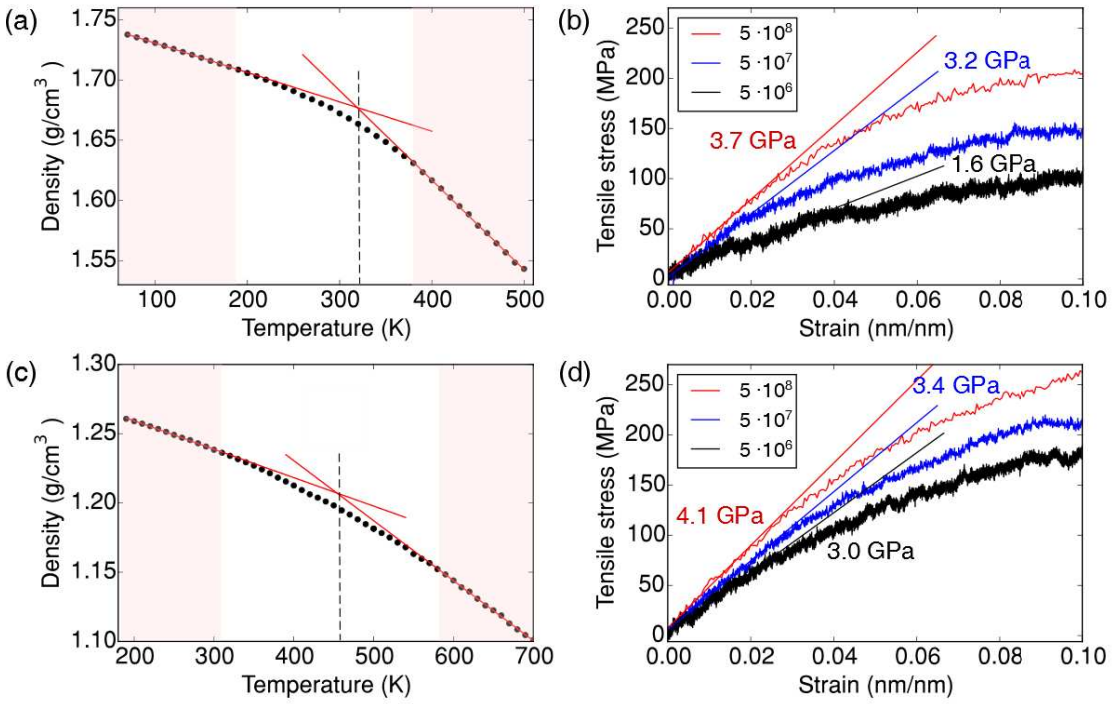


**Figure 5.** Density as a function of temperature (a,c) and tensile stress-strain curves (b,d) for PVDF (a,b) and epoxy (c,d). The glass transition temperature is estimated as the intersection of the linear fits (fitted regions shaded) of the lower and higher temperature areas (red lines in a,c).

The elastic moduli of three different strain rates are calculated in the linear range up to 2 % strain (lines in b,d). The strain rates in the legends are given in $s^{-1}$.

The evolution of the PVDF density with temperature is reported in Figure 5a. Linear fits in the lower and higher temperature regions indicate a glass transition temperature $T_g \approx 320$ K, which should be compared with the experimental value of about 230 K. The overestimation of $T_g$ is not uncommon and is due to the low chain mobility during the short MD runs in which the density is optimized, which do not give the chains sufficient time to relax completely. Nevertheless, the deviation from the experimental value is still acceptable and comparable to values obtained for thermoplastic polymers with similar methods[15]. The predicted density at 300 K (1.68 g/cm$^3$) is only slightly lower than the experimental density of 1.78 g/cm$^3$,[23] in part because of the lack of crystalline regions and in part because the shorter chains possess a larger free volume at the chain ends.

The predicted stress-strain curves at three different strain rates are reported in Figure 5b. Linear fits up to a strain of 2% leads to Young's moduli between 1.6 and 3.7 GPa, which compare very favourably with experimental values around 2.6 GPa[24].

As far as the thermoset component is concerned, the cross-linking procedure after relaxation of the liquid mixture of the three epoxy molecules and the curing agent led to a saturated conversion value of about 95% (Figure 6a). This is calculated as the ratio of reacted N sites and the maximum available sites. It should be noted that, due to the resin composition, there are about 1.5 times more reactive carbon sites than nitrogen sites.

A conversion of 95 % thus means that only 63 % of all available carbon sites have undergone a cross-linking reaction. The non-monotonous evolution of the conversion with the number of cross-linking cycles is due to the increment of the cross-linking cutoff distances after cycles 11

and 21, as explained in the Methods section. The slightly lower conversion of secondary bonds with respect to primary bonds in Figure 6a is clear, although the curves follow the same trend and converge to roughly the same value at saturation. A representative snapshot of portion of a cross-linked network is shown in Figure 6b.

The predicted $T_g$ of 455 K (Figure 5c) and Young's moduli between 3 and 4 GPa (Figure 5d) at the considered strain rates agree remarkably well with values of typical epoxy resins at high cross-linking conversion (476 K and 3.5 GPa for a commercial multicomponent resin[25]). As articulated earlier, since the cooling rate implemented in our simulations is several orders of magnitude faster than the experimentally accessible cooling rates, a discrepancy between the calculated and experimental $T_g$ values is expected.

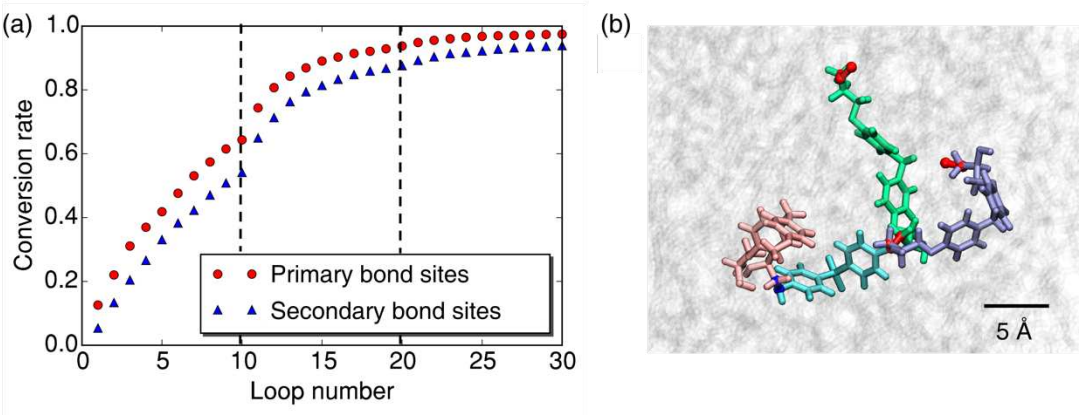


**Figure 6.** (a) Conversion of primary and secondary bond sites as a function of secondary bond cycle number. Each ten loops the cutoff distances are incremented by 0.5 Å. (b) Molecular detail of the cross-linking between DDS (cyan) and three BIS molecules (green, ice-blue, pink). Blue and red bonds depict primary and secondary cross-linked sites, respectively.

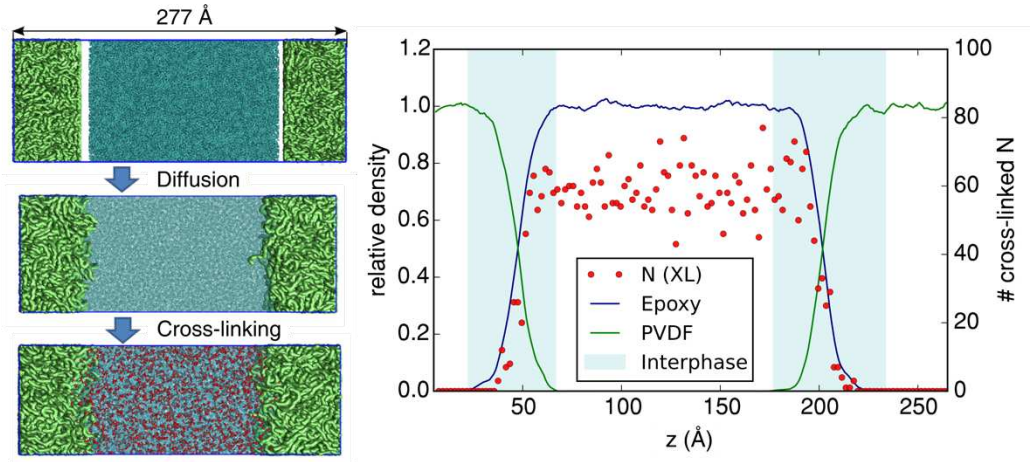


**Figure 7.** Left*:* Scheme of the interface generation procedure. PVDF molecules: green, Epoxy molecules: cyan, cross-linked sites: red. Right: Final distribution of cross-linked nitrogen atoms at 93% of total conversion along the *z* axis perpendicular to the interfaces, averaged in 2Å-wide intervals (red dots) superimposed to the density profiles of PVDF and Epoxy normalized to their bulk densities at 500 K (1.55 g/cm$^3$ and 1.05 g/cm$^3$, respectively)

**3.2. Thermoplastic/thermoset interface.** Having ensured a reasonable prediction of bulk properties for both PVDF and the epoxy phases, an interface model system was then created with both phases in a common simulation cell. The epoxy liquid phase was prepared as before, with the four molecular components intermixed and the density of this mixture optimized using the rescaling option. Rescaling was carried out with periodic boundary conditions applied to the *x* and *y* directions, but not the *z* direction perpendicular to the hybrid interface. In the z direction molecules were restrained from passing the boundary by the action of two dynamically moving Lennard-Jones planar walls that were oriented parallel to the upper and the lower faces of the

(<- p. 3987)

simulation cell (LAMMPS *wall* command). The so-obtained slab was then placed in a large simulation cell. The PVDF phase was created starting from a non-periodic input file to obtain clean PVDF surfaces to be initially interfaced with the epoxy phase (Figure 7, left). This was

realized by first placing PVDF chains in their unwrapped state in a very large simulation cell (see S.I., Figure S7). Then a slab was created by a reduction of the density with help of Lennard-Jones walls in the z direction as described above for the epoxy system. The so-obtained thermoplastic slab was placed near the epoxy slab with an initial distance of ca. 5 Å between the surfaces in the *z* direction, resulting in a simulation cell with initial dimensions of 10.2 × 11.0 × 27.7 $nm^3$.

At this point, the combined system was relaxed employing the already described 21-step (<- p. 3988) equilibration protocol following Abbott et al.[16]. This scheme was designed specifically to overcome the energy barriers associated with the translation and rotation of the monomers in each TP chain and reach a uniform equilibrium density within reasonable simulation times, by applying unphysically high peak temperatures and pressures (1000 K and $5 \cdot 10^4$ bar, respectively) before cooling and relaxing to the desired final state (in our case, 500 K and 1 bar). As stated earlier, in the case of bulk PVDF the application of this protocol was not crucial to obtain a reasonably good model of the thermoplastic melt (see Table 1). In the case of the interfacial system, however, the accelerated equilibration at several consecutive steps of high temperatures and pressures is precisely what is needed to generate a well inter-penetrated interphase between PVDF and the liquid epoxy precursor (Figure 7), at the expenses of knowledge about the true time associated with the inter-diffusion process.

Only at this stage, after 21-step equilibration, was the cross-linking between the epoxide monomers and the curing agent activated, following the same conversion cycles as before (see Figures 3 and 6). As a result, we obtained a dense and cross-linked PVDF/epoxy/PVDF system periodically repeated in all directions, as shown in Figure 7. The profiles of the densities of the two phases integrated in *xy* planes show that the interphase regions extend over about 5 nm and

are separated by sufficiently large bulk regions of the pure components (Figure 7). The interphase can be unambiguously defined as the space in *z* direction where neither the epoxy nor the PVDF component has a zero density. Superimposed on the density profiles is the number of cross-linked N atoms (red dots in the graphic in Figure 7), at the saturation conversion of 93%. These results indicate that the cross-link bonds were not only created uniformly across the whole epoxy body, but also extend into most of the interphase volume.

The formation of a cross-linked epoxy network deep into the TP region means that there is a high probability of forming mutually interpenetrating chain loops that lock the two phases together *via* topological constraints of their molecular structures. In fact, a qualitative search for the formation of such loops immediately revealed a number of them, as illustrated in the example provided in Figure 8. Such loops are the result of the epoxy cross-linking taking place into and around the interfacial PVDF chains, which have entered the epoxy phase *via* thermal activation of their mobility during co-curing. The formation of mutually entangled loops at hybrid polymer interfaces is the characteristic feature of so-called semi-interpenetrating polymer networks (semi-IPN). The interlocking of PVDF molecules in the cross-linked epoxy network is expected to be a major contributor towards a very strong interfacial adhesion, owing to the extended interphase between the TS and TP components.

As a first, qualitative estimation of the interfacial strength, we modelled the behavior of the hybrid TS/TP system under tensile strain at a strain rate of $5 \cdot 10^{7}$ $s^{-1}$ (Figure 9). In the low-strain linear region of the stress-strain curve, the elasticity of the hybrid system can be well described by a linear superposition of the separate components. Indeed, the Young modulus obtained by linear fit of the curve up to 2% strain (3.5 GPa) agrees well with the modulus of mixing computed from the moduli of the bulk components weighted by their volume fractions:

$$E_{interphase} = E_{PVDF}\ \varphi + E_{epoxy}\ (1 - \varphi)$$

In our system, φ is 0.41, leading to $E_{interphase}$ = 3.3 GPa.

Increasing the strain up to 45% caused no noticeable failure at the interface or in the bulk components (Figure 9a), while the stress curve deviated from the linear elastic regime (Figure 9b). It should be noted that experimental systems tested with inter-laminar shear tests fail at much lower strain (of the order of 2 to 5%) due to the presence of critical defects of characteristic sizes much larger than our simulation system. Failure might occur due to weaknesses between non-bonded polymer chains, covalent bond breakage, or both. It should be noted that the force-field used in our simulations cannot capture dynamic bond breakage events. However, what our simulations tell us is that even at very high strain levels, a perfectly entangled interface can remain strongly adhered and does not show signs of incipient failure.

The onset of failure takes place at 49.8 % strain at the edge of the interphase region at the PVDF side (see snapshots in Figure 9a). The presence of not entirely cross-linked epoxy molecules in the immediate neighborhood of the growing void is a notable feature (Figure 9c). Further increasing the strain causes evident pull-out of individual PVDF chains, that unwind from the TP bulk while still remaining locked into the epoxy resin at the opposite side of the interface (Figure 10).

The observed failure behavior is therefore correlated with the presence of numerous mutually entangled loops such as the one shown in Figure 8. Even in the absence of covalent bonding between the epoxy molecules and the PVDF chains, such high degree of entanglement (shown in Figure 10) may confer an interfacial adhesion almost as strong as the cohesion within bulk PVDF itself.

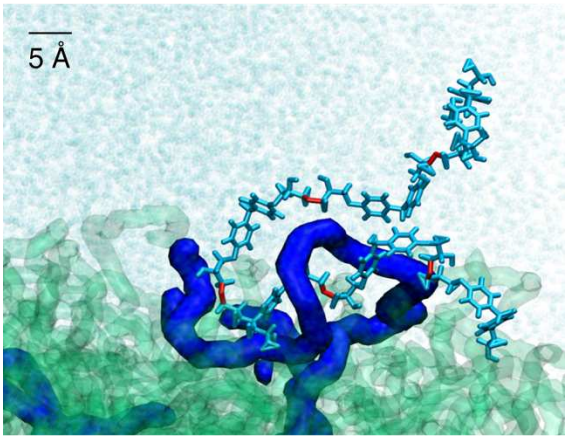


**Figure 8.** A pair of mutually entangled loops between a PVDF chain (highlighted as a blue tube) and a cross-linked molecular pathway within epoxy (cyan sticks, red bonds), obtained after simulated co-curing and cooling to 300 K.

## 4. DISCUSSION

**4.1. Advantages and limitations of the model systems.** All-atom molecular dynamics techniques present obvious limitations when employed to study polymer materials, especially thermoplastics. Neither their complex microstructural features, for example partial crystallinity[24], nor their dynamical behaviour spanning a multitude of time scales can be addressed with current code implementations and computer architectures.

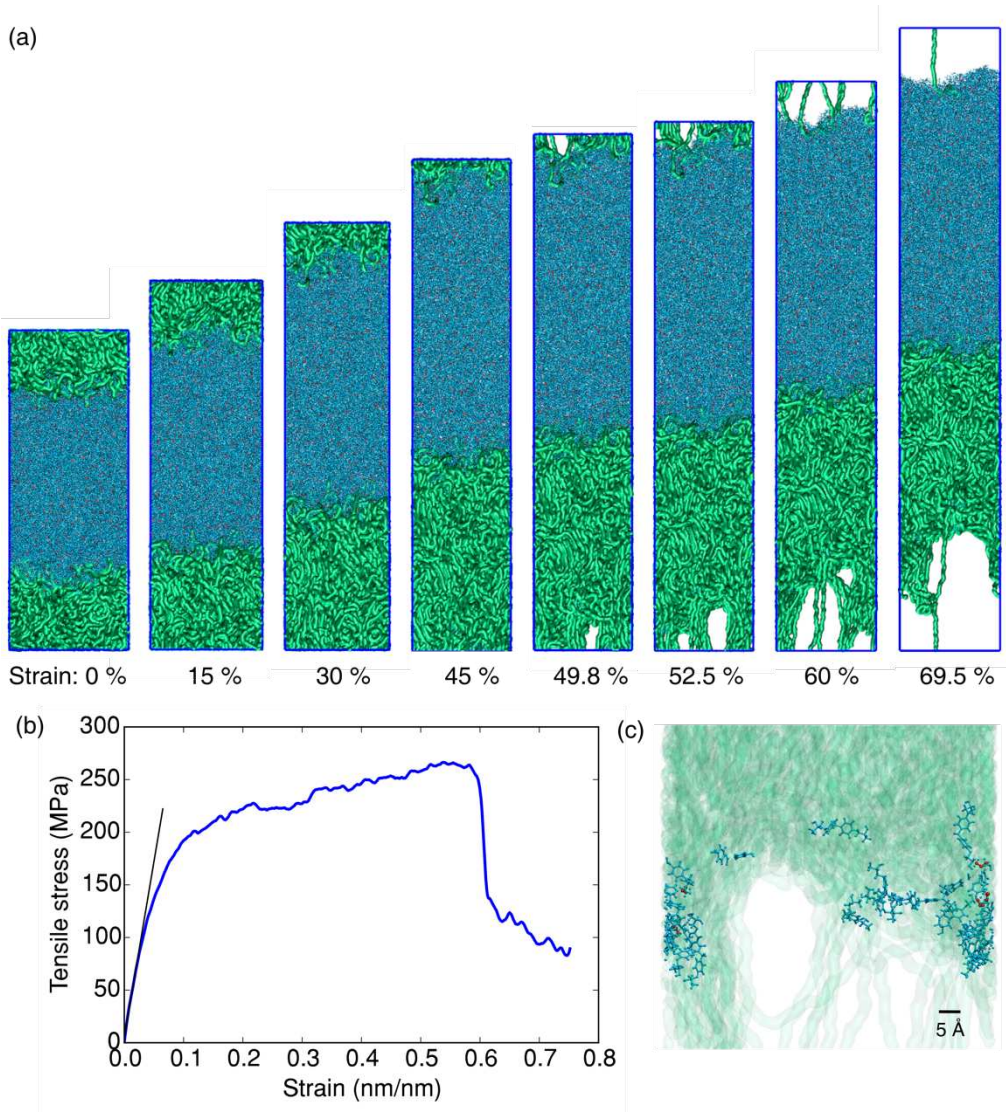


**Figure 9.** (a) Snapshots of a MD simulation of the fracture of the interface system under tensile strain (indicated in % under each snapshots). (b) Corresponding stress-strain curve. (c) Details of the failed interface at 55% strain, showing that epoxy molecules (cyan) remain trapped within the stressed PVDF matrix (green).

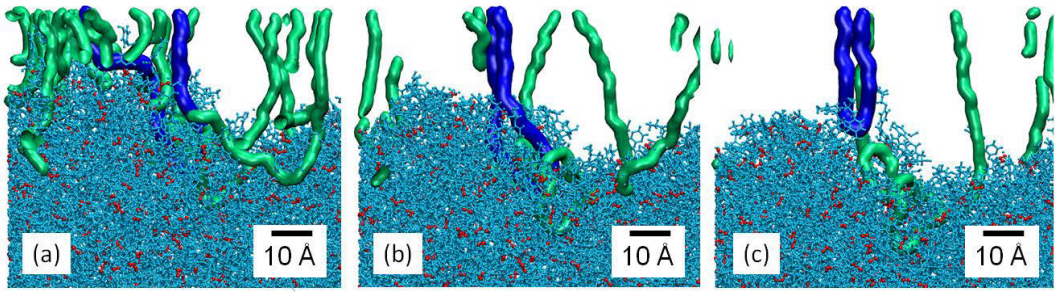


**Figure 10.** Pull-out of a PVDF loop (highlighted in blue) tightly intertwined with the cross-linked epoxy phase during interface failure at large tensile strain (55-60%). The color scheme is described in Fig. 7.

For this reason, all-atom models with chain lengths of about 100 repeat units represent the state of the art[15], with much smaller oligomer models being the standard until recent times[27,28]. The use of short chains, however, presents the advantage that realistic structural and thermo-mechanical properties can be computationally predicted in shorter times due to a compensation of errors. For instance, the glass transition temperature is much smaller for shorter chains than for longer chains. However, since the simulated cooling rate used to obtain density/temperature curves is typically orders of magnitude greater than the experimental cooling rates, we have been able to obtain reasonable agreement between experimental and predicted values (Figure 5). Similar considerations hold for the prediction of elastic moduli taking into account the much larger strain rates used in the simulations.

(<- p. 3989)

That said, in the present work we did not seek a quantitatively accurate prediction of thermo-mechanical properties. These are, for technological polymeric materials, determined more by the nature and amount of additives rather than by the intrinsic properties of the pure polymers. While PVDF is also available as high-purity homopolymer (e.g. Kynar®) epoxy resins, for instance, are always made more compliant by the addition of softeners, which are not considered in our model

systems. In contrast, our systems were purposely constructed with the aim of providing previously unknown atomic-level insights into the structure of hybrid TS/TP interfaces. The aim of our work is to provide practical guidance for engineers to optimize process steps (in our specific case: co-curing) with a better understanding of the system's chemical features.

Nevertheless, it is reassuring that our computationally predicted values of the density at 300 K, Flory's characteristic ratio $C_\infty$, glass transition temperature $T_g$ and elastic modulus $E$ are well within the range of typical experimental values, and that the observed deviations can be readily ascribed to the system-size and simulation-time limitations, as mentioned above. It must be also stressed that some degree of subjectivity is always present, since different choices of the regions in which the density/temperature and stress/strain curves are fitted with linear regressions may impact the predicted $T_g$ and $E$ values by as much as 20 to 50%.

(<- p. 3990)

A crucial aspect of our simulations is the protocol employed to cross-link the epoxy molecule with the curing agent. The procedure is conceived in a way that a realistic topology of the network (conversion, density, branching) can be obtained without explicit consideration of true reaction rates and diffusion[14]. The algorithm used in this work has been validated in a number of previous studies[14,29-32]. It is reasonably simple, efficient, and can be implemented *via* the use of LAMMPS internal scripts to perform polymerization and topology updates 'on the fly' during MD simulation runs. As an extension of the algorithm used in the present study, a Monte-Carlo step in addition to the distance cut-off criterion could be implemented to account for the different reactivity of chemically different components, if wished. However, this was not necessary in the present work.

**4.2. Details of the hybrid TS/TP interface.** In the current literature to date, no atomistic model has been ever proposed for hybrid thermoset/thermoplastic interfaces produced by co-

curing. The model that we have obtained in this work relies on two features: First, the capability of the 21-step equilibration to promote diffusion of the thermoplastic chains in the liquid epoxy mixture. Second, it relies on the ability of the cross-linking procedure to generate an epoxy network even at the lowest concentrations of molecules deeply buried in the PVDF phase. Several simulation parameters can be tuned to control the degree of interpenetration of the two matrices. The first is the total time spent during the TP equilibration, which exerts a direct influence on the width of the interphase region, provided that the two phases are well miscible. In our case, an interphase width of about 5 nm was obtained with the pristine 21-step protocol[16]. In additional test simulations, a ten-times longer equilibration time led to a threefold increase of the width (see S.I., Figure S9). In reality, the interphase itself spans much larger distances, of the order of 10 μm (see Figure 1, left), so that a full-size atomic-scale modelling of all of its features is beyond our current capabilities. Being primarily interested in the potential formation of a semi-interpenetrating polymer network (semi-IPN), the system size and short equilibration time used here are acceptable.

The temperature and pressure values in the individual steps of the equilibration could also be varied as needed. At this stage, we have not performed a systematic study of how these affect the interfacial properties. That said, we observed that excessive pressures acted against the growth of the semi-IPN features, because the PVDF chains were less able to escape the bulk and form open loops within the epoxy liquid. However, identification of which parameters are closer to the experimental reality is very difficult to assess, given that the stepwise, abrupt changes of temperature and pressure do not allow for quantification of diffusion coefficients of the interfaced components. In fact, our procedure is specifically designed to avoid explicit consideration of diffusion. Experimental characterization of the interfacial roughness at the nm-

scale, if possible, would provide a means for comparison against our obtained structures (see S.I., Figure S8), but has yet to be reported. As a further improvement of the simulation procedure, numerical solutions of reaction-diffusion equations parametrized so as to reproduce experimental details of the interphase geometry (e.g. its thickness) could be employed to augment the MD results with quantification of the so far not accessible process kinetics. This is required for instance to assess the extent of miscibility and the depth of interpenetration of the TP and TS components during co-curing.

The formation of mutually entangled loops between PVDF chains and the cross-linked epoxy matrix is perhaps the most intriguing and compelling feature predicted by our simulations. Our findings indicate that the interface may be mechanically as strong as pure PVDF, even in the absence of covalent bond formation between the reactive sites of the epoxy molecules and PVDF. Formation of such bonds is theoretically possible, and will be worth investigating in future studies, given that the cross-linking conversion is not fully saturated in the interphase region and that the polarity of the PVDF chains may promote chemical attack by the terminal epoxy rings.

To date, comparable experimental data remain to be reported, and therefore our analyses are qualitative as far as the predicted entangled topology is concerned. Nonetheless, a more quantitative characterization could be performed in future to analyse the entanglement density, for instance by mean of primitive path analysis[33]. Also, it could be interesting to model the interpenetration of PVDF into the epoxy liquid precursor and at the same time its gelation due to cross-linking[34], in order to study kinetics effects due to the balance between conversion rate and diffusion.

**4.3. Interface strength.** As mentioned above, we ascribe the entangled loops depicted in Figure 8 to the interfacial strength, which we have addressed here by applying a constant strain rate in direction perpendicular to the interface to our model system. At low strains, elongation follows linear elasticity, with a viscoelastic contribution visible in the variability of the Young modulus with the applied strain rate. In our model the resin is only slightly viscoelastic, but it should be noted that experimental resin formulations typically include softeners that strongly affect their mechanical properties. Also, we note that the quantification of the elastic response of our models relies on the harmonic DREIDING force-field parameters, which is reasonable and robust in the linear-elastic regime but may be too simplistic at the highest strain conditions explored in our simulations.

As a compelling indication of the strength of the interface, no failure of the system took place up to elongations that are ten times greater than those sustained by real systems. We propose this is due to the small simulated system size, which prevents the inclusion of critical defects, from which cracks can nucleate. We found that incipient failure was accompanied by chain pull-out, a typical behaviour of thermoplastic systems, which has been reported before in coarse-grained simulations of a heterogeneous TP/TP interface[33].

It remains an open question how the putative formation of covalent bonds between PVDF and the epoxy would further strengthen the interfacial adhesion properties. Such bonds would certainly prevent chain pull-out from the epoxy network. We therefore expect that, in the absence of microscopic sources of stress concentration extraneous to the polymer components, fracture would not preferentially occur or propagate along the hybrid interface.

## 5. CONCLUSIONS

In summary, our computational procedure for modeling the formation of a hybrid TP/TS interface recovered features of inter-diffusion, semi-IPN formation, and chain pull-out upon tensile deformation of the interphase. However, diffusion could not be tracked quantitatively, and the competition of diffusion and cross-linking could not be evaluated. Based on our interphase model generated in this work, the complexity of the system may be further increased by consideration of chemical reactivity between the TS and TP molecules. Moreover, chemically predictive simulation techniques may be used to further investigate the possible mechanisms of interfacial failure, taking into account critical crack propagation associated with breakage of covalent bonds. Moreover, future studies could benefit by improvements in terms of addressing challenges associated with simulation timescale. Specifically, this could be achieved for example by multi-scale modelling employing united-atom approaches[35] or coarse grain models[33,34]. However, as these models would average over atomistic properties that could be essential to properly describe the heterogeneous interface, the use of all-atom benchmarks will be essential. In particular, the issue of remapping from a coarse-grained onto a correct atomistic representation should be addressed with great care.

(<- p. 3991)

## ASSOCIATED CONTENT

The supporting information includes Table S1, Figures S1, S2, S3, S4, S5, S6, S7, S8, S9. Parameters for partial charge calculation are listed and partial charges displayed for all atoms involved. Figures are included that further illustrate the structure generation of bulk and slab PVDF and bulk epoxy. Interphase roughness and data for enhanced interfacial diffusion are shown.

## AUTHOR INFORMATION


### Contact Author

*Corresponding author. E-Mail: colombi@hmi.uni-bremen.de. Tel. +49 421 21864570.


### Notes

The authors declare no competing financial interest.

## ACKNOWLEDGEMENTS


This project has been supported by the German Bundesministerium für Bildung und Forschung under Grant No. 03ZZ0621B, and by the Australian Research Council under grant DP140100165. Computational resources have been provided by the North-German Supercomputing Alliance (HLRN). We are grateful to Steffen Lid (University of Bremen) for suggestions and assistance regarding the LAMMPS implementation of the simulated cross-linking scheme.


## REFERENCES


(1) Soutis, C. Carbon Fiber Reinforced Plastics in Aircraft Construction. *Mater. Sci. Eng. A* **2005**, *412* (1), 171–176. DOI: 10.1016/j.msea.2005.08.064.

(2) Tsao, C. C.; Hocheng, H. Analysis of Delamination in Drilling Composite Materials by Core-Saw Drill. *Int. J. Mater. Prod. Technol.* **2008**, *32* (2–3), 188–201. DOI: 10.1504/IJMPT.2008.01898.

(3) Ageorges, C.; Ye, L.; Hou, M. Advances in Fusion Bonding Techniques for Joining Thermoplastic Matrix Composites: A Review. *Compos. Part Appl. Sci. Manuf.* **2001**, *32* (6), 839–857. DOI: 10.1016/S1359-835X(00)00166-4.

(4) Don, C. R.; McKnight, S. H.; Wetzel, E. D.; Gillespie Jr, W. J. Application of Thermoplastic Resistance Welding Techniques to Thermoset Composites. Proceedings of the ANTEC 94, 1994.

(5) Hou, M. Thermoplastic Adhesive for Thermosetting Composites. *Mater. Sci. Forum* **2012**, *706–709*, 2968–2973. DOI: 10.4028/www.scientific.net/MSF.706-709.2968.

(6) Dumont, D.; Seveno, D.; De Coninck, J.; Bailly, C.; Devaux, J.; Daoust, D. Interdiffusion of Thermoplastics and Epoxy Resin Precursors: Investigations Using Experimental and Molecular Dynamics Methods. *Polym. Int.* **2012**, *61* (8), 1263–1271. DOI: 10.1002/pi.4201.

(7) Plimpton, S. Fast Parallel Algorithms for Short-Range Molecular Dynamics. *J. Comput. Phys.* **1995**, *117* (1), 1–19. DOI: 10.1006/jcph.1995.1039.

(8) Mayo, S. L.; Olafson, B. D.; Goddard, W. A. DREIDING: A Generic Force Field for Molecular Simulations. *J Phys Chem* **1990**, *94*, 8897–8909. DOI: 10.1021/j100389a010.

(9) Nosé, S. A Unified Formulation of the Constant Temperature Molecular Dynamics Methods. *J. Chem. Phys.* **1984**, *81* (1), 511–519. DOI: 10.1063/1.447334.

(10) Hoover, W. G. Canonical Dynamics: Equilibrium Phase-Space Distributions. *Phys. Rev. Gen. Phys.* **1985**, *31* (3), 1695–1697. DOI: 10.1103/PhysRevA.31.1695.

(11) Hoover, W. G. Constant-Pressure Equations of Motion. *Phys. Rev. A* **1986**, *34* (3), 2499–2500. DOI: 10.1103/PhysRevA.34.2499.

(12) Hockney, R. W.; Eastwood, J. W. *Computer Simulation Using Particles*; New York: McGraw-Hill, 1981.

(13) Rappe, A. K.; Goddard, W. A. Charge Equilibration for Molecular Dynamics Simulations. *J. Phys. Chem.* **1991**, *95* (8), 3358–3363. DOI: 10.1021/j100161a070.

(14) Demir, B.; Walsh, T. R. A Robust and Reproducible Procedure for Cross-Linking Thermoset Polymers Using Molecular Simulation. *Soft Matter* **2016**, *12* (8), 2453–2464. DOI: 10.1039/C5SM02788H.

(15) Haley, B. P.; Li, C.; Wilson, N.; Jaramillo, E.; Strachan, A. Atomistic Simulations of Amorphous Polymers in the Cloud with PolymerModeler. arXiv:1503.03894.

(16) Abbott, L. J.; Hart, K. E.; Colina, C. M. Polymatic: A Generalized Simulated Polymerization Algorithm for Amorphous Polymers. *Theor. Chem. Acc.* **2013**, *132* (3), 1–19. DOI: 10.1007/s00214-013-1334-z.

(17) Hofmann, D.; Fritz, L.; Ulbrich, J.; Schepers, C.; Böhning, M. Detailed-Atomistic Molecular Modeling of Small Molecule Diffusion and Solution Processes in Polymeric Membrane Materials. *Macromol. Theory Simul.* **2000**, *9* (6), 293–327. DOI: 10.1002/1521-3919(20000701)9:6%3C293::AID-MATS293%3E3.0.CO;2-1.

(18) Larsen, G. S.; Lin, P.; Hart, K. E.; Colina, C. M. Molecular Simulations of PIM-1-like Polymers of Intrinsic Microporosity. *Macromolecules* **2011**, *44* (17), 6944–6951. DOI: 10.1021/ma200345v.

(19) Hanwell, M. D.; Curtis, D. E.; Lonie, D. C.; Vandermeersch, T.; Zurek, E.; Hutchison, G. R. Avogadro: An Advanced Semantic Chemical Editor, Visualization, and Analysis Platform. *J. Cheminformatics* **2012**, *4*, 17. DOI: 10.1186/1758-2946-4-17.

(20) Martínez, L.; Andrade, R.; Birgin, E. G.; Martínez, J. M. PACKMOL: A Package for Building Initial Configurations for Molecular Dynamics Simulations. *J. Comput. Chem.* **2009**, *30* (13), 2157–2164. DOI: 10.1002/jcc.21224.

(21) Rubinstein, M.; Colby, R. H. *Polymer Physics*; OUP Oxford, 2003.

(22) Lutringer, G.; Weill, G. Solution Properties of Poly(Vinylidene Fluoride): 1. Macromolecular Characterization of Soluble Samples. *Polymer* **1991**, *32* (5), 877–883. DOI: 10.1016/0032-3861(91)90514-J.

(23) Material Data Center. Datasheet Kynar® 710 https://www.materialdatacenter.com/ms/en/tradenames/Kynar/ARKEMA/ (accessed Oct 20, 2017).

(24) Lynch, C. S. Polyvinylidene Fluoride (PVDF) Elastic, Piezoelectric, Pyroelectric, and Dielectric Coefficients and Their Non-Linearities. *Ferroelectrics* **1993**, *150* (1), 331–342. DOI: 10.1080/00150199308211451.

(25) HEXCEL. HexPly® M21 Epoxy Matrix Product Data (180°C/356°F Curing Matrix). Hexcel Publication FTA002c March 2007.

(26) Okada, O.; Oka, K.; Kuwajima, S.; Toyoda, S.; Tanabe, K. Molecular Simulation of an Amorphous Poly(Methyl Methacrylate)–poly(Tetrafluoroethylene) Interface. *Comput. Theor. Polym. Sci.* **2000**, *10* (3), 371–381. DOI: 10.1016/S1089-3156(00)00002-7. (<- p. 3992)

(27) Charati, S. G.; Stern, S. A. Diffusion of Gases in Silicone Polymers: Molecular Dynamics Simulations. *Macromolecules* **1998**, *31* (16), 5529–5535. DOI: 10.1021/ma980387e.

(28) Ayyagari, C.; Bedrov, D.; Smith, G. D. Structure of Atactic Polystyrene: A Molecular Dynamics Simulation Study. *Macromolecules* **2000**, *33* (16), 6194–6199. DOI: 10.1021/ma0003553.

(29) Demir, B.; Henderson, L. C.; Walsh, T. R. Design Rules for Enhanced Interfacial Shear Response in Functionalized Carbon Fiber Epoxy Composites. *ACS Appl. Mater. Interfaces* **2017**, *9* (13), 11846–11857. DOI: 10.1021/acsami.6b16041.

(30) Servinis, L.; Beggs, K. M.; Gengenbach, T. R.; Doeven, E. H.; Francis, P. S.; Fox, B. L.; Pringle, J. M.; Pozo-Gonzalo, C.; Walsh, T. R.; Henderson, L. C. Tailoring the Fibre-to-Matrix Interface Using Click Chemistry on Carbon Fibre Surfaces. *J. Mater. Chem. A* **2017**, *5* (22), 11204–11213. DOI: 10.1039/C7TA00922D.

(31) Demir, B.; Beggs, K.; Fox, B.; Servinis, L.; Henderson, L.; R. Walsh, T. A Predictive Model of Interfacial Interactions between Functionalised Carbon Fibre Surfaces Cross-Linked with Epoxy Resin. *Compos. Sci. Technol.* **2018**. DOI: 10.1016/j.compscitech.2018.02.029.

(32) Eyckens, D. J.; Servinis, L.; Scheffler, C.; Wölfel, E.; Demir, B.; Walsh, T. R.; Henderson, L. C. Synergistic Interfacial Effects of Ionic Liquids as Sizing Agents and Surface Modified Carbon Fibers. *J. Mater. Chem. A* **2018**, *6* (10), 4504–4514. DOI: 10.1039/C7TA10516A.

(33) Ge, T.; Grest, G. S.; Robbins, M. O. Tensile Fracture of Welded Polymer Interfaces: Miscibility, Entanglements, and Crazing. *Macromolecules* **2014**, *47* (19), 6982–6989. DOI: 10.1021/ma501473q.

(34) Li, M.; Gu, Y.-Z.; Li, Y.-X.; Liu, H.; Zhang, Z.-G. Competition of Diffusion and Crosslink on the Interphase Region in Carbon Fiber/Epoxy Analyzed by Multiscale Simulations. *J. Appl. Polym. Sci.* **2014**, *131* (7), n/a-n/a. DOI: 10.1002/app.40032.

(35) Hossain, D.; Tschopp, M. A.; Ward, D. K.; Bouvard, J. L.; Wang, P.; Horstemeyer, M. F. Molecular Dynamics Simulations of Deformation Mechanisms of Amorphous Polyethylene. *Polymer* **2010**, *51* (25), 6071–6083. DOI: 10.1016/j.polymer.2010.10.009.
(<- p. 3993)

TOC graphic:

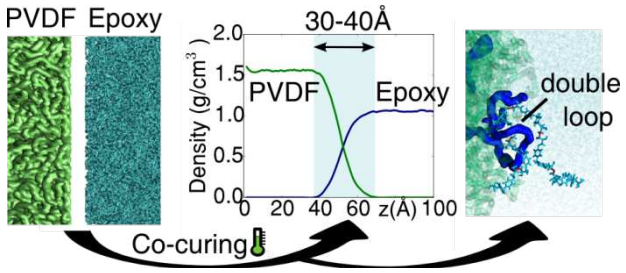
PVDF
Epoxy
30-40Å
2.0
1.5
1.0
0.5
0.0
Density (g/cm3)
PVDF
Epoxy
0
20
40
60
z(Å)
100
double
loop
Co-curing

and 21, as explained in the Methods section. The slightly lower conversion of secondary bonds with respect to primary bonds in Figure 6a is clear, although the curves follow the same trend and converge to roughly the same value at saturation. A representative snapshot of portion of a cross-linked network is shown in Figure 6b.

The predicted $T_g$ of 455 K (Figure 5c) and Young's moduli between 3 and 4 GPa (Figure 5d) at the considered strain rates agree remarkably well with values of typical epoxy resins at high cross-linking conversion (476 K and 3.5 GPa for a commercial multicomponent resin[25]). As articulated earlier, since the cooling rate implemented in our simulations is several orders of magnitude faster than the experimentally accessible cooling rates, a discrepancy between the calculated and experimental $T_g$ values is expected.

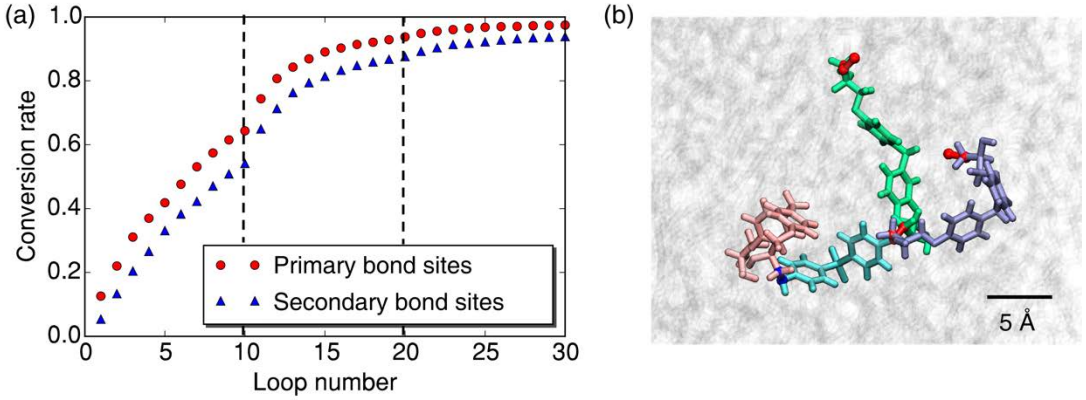


**Figure 6.** (a) Conversion of primary and secondary bond sites as a function of secondary bond cycle number. Each ten loops the cutoff distances are incremented by 0.5 Å. (b) Molecular detail of the cross-linking between DDS (cyan) and three BIS molecules (green, ice-blue, pink). Blue and red bonds depict primary and secondary cross-linked sites, respectively.

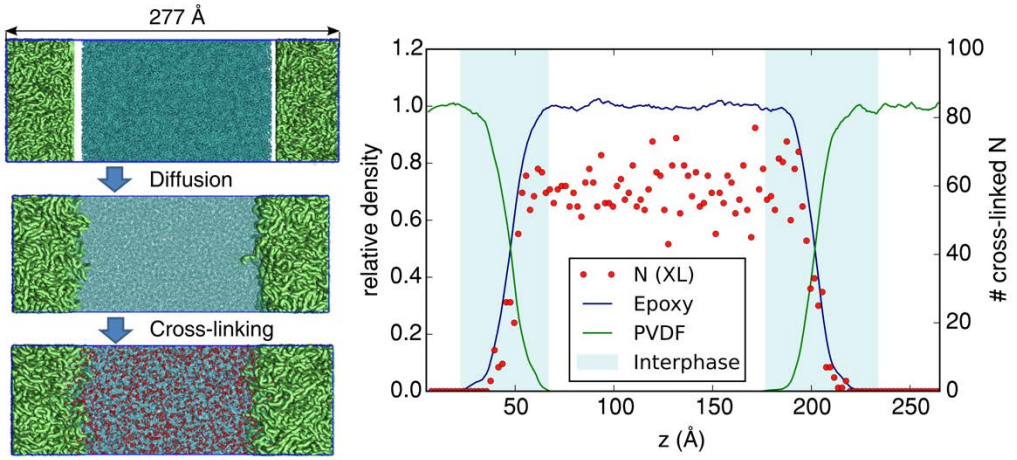


**Figure 7.** Left*:* Scheme of the interface generation procedure. PVDF molecules: green, Epoxy molecules: cyan, cross-linked sites: red. Right: Final distribution of cross-linked nitrogen atoms at 93% of total conversion along the *z* axis perpendicular to the interfaces, averaged in 2Å-wide intervals (red dots) superimposed to the density profiles of PVDF and Epoxy normalized to their bulk densities at 500 K (1.55 g/cm$^3$ and 1.05 g/cm$^3$, respectively)

**3.2. Thermoplastic/thermoset interface.** Having ensured a reasonable prediction of bulk properties for both PVDF and the epoxy phases, an interface model system was then created with both phases in a common simulation cell. The epoxy liquid phase was prepared as before, with the four molecular components intermixed and the density of this mixture optimized using the rescaling option. Rescaling was carried out with periodic boundary conditions applied to the *x* and *y* directions, but not the *z* direction perpendicular to the hybrid interface. In the z direction molecules were restrained from passing the boundary by the action of two dynamically moving Lennard-Jones planar walls that were oriented parallel to the upper and the lower faces of the

(<- p. 3987)

simulation cell (LAMMPS *wall* command). The so-obtained slab was then placed in a large simulation cell. The PVDF phase was created starting from a non-periodic input file to obtain clean PVDF surfaces to be initially interfaced with the epoxy phase (Figure 7, left). This was

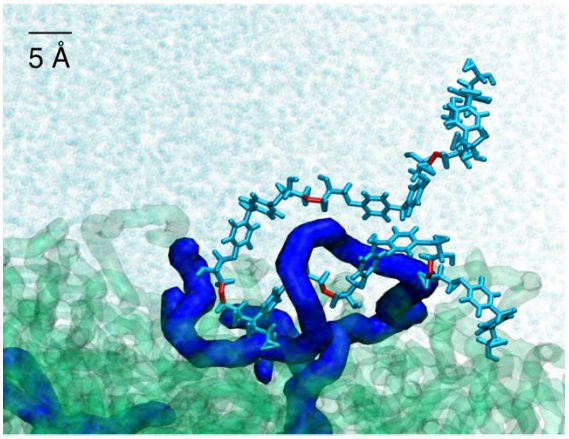


**Figure 8.** A pair of mutually entangled loops between a PVDF chain (highlighted as a blue tube) and a cross-linked molecular pathway within epoxy (cyan sticks, red bonds), obtained after simulated co-curing and cooling to 300 K.

## 4. DISCUSSION

**4.1. Advantages and limitations of the model systems.** All-atom molecular dynamics techniques present obvious limitations when employed to study polymer materials, especially thermoplastics. Neither their complex microstructural features, for example partial crystallinity[24], nor their dynamical behaviour spanning a multitude of time scales can be addressed with current code implementations and computer architectures.

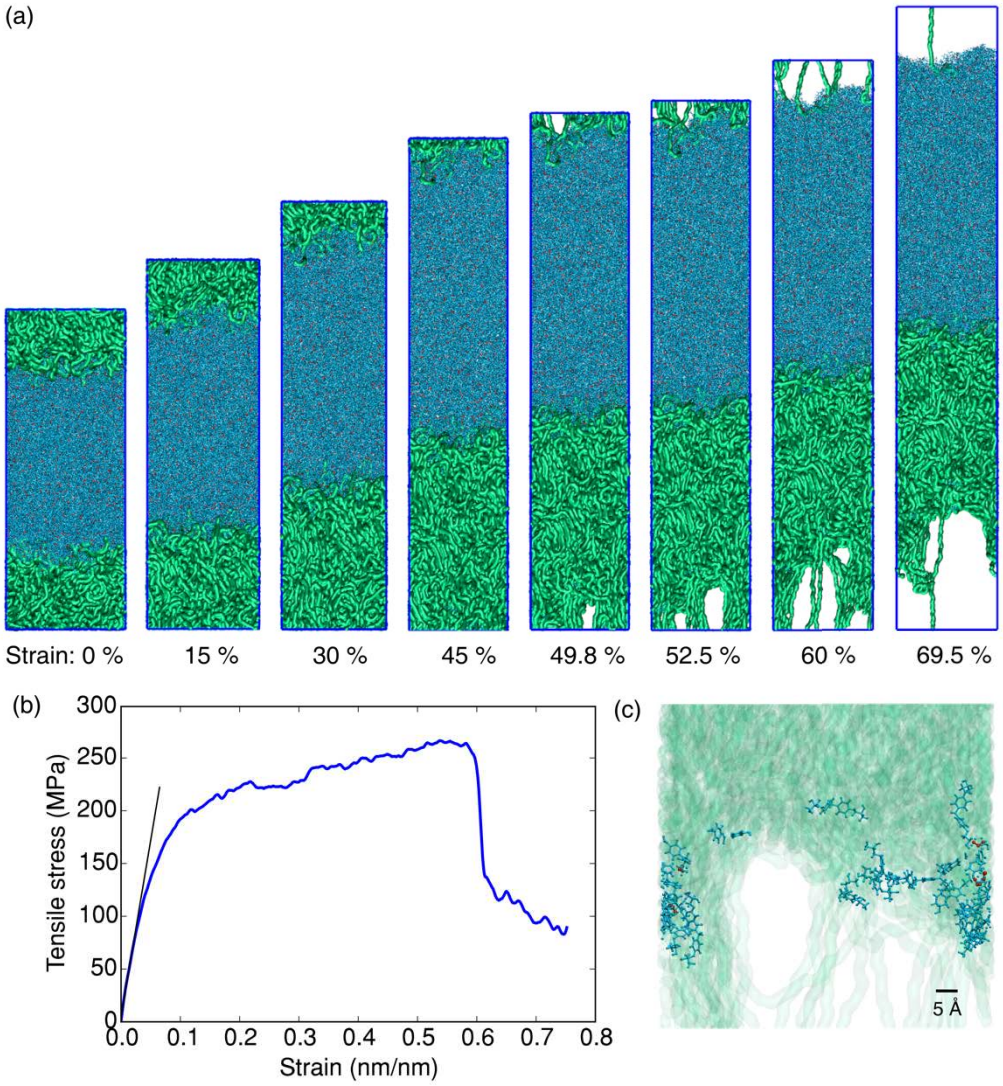


**Figure 9.** (a) Snapshots of a MD simulation of the fracture of the interface system under tensile strain (indicated in % under each snapshots). (b) Corresponding stress-strain curve. (c) Details of the failed interface at 55% strain, showing that epoxy molecules (cyan) remain trapped within the stressed PVDF matrix (green).

TOC graphic:

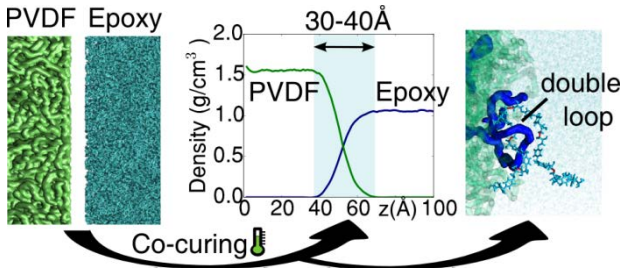
PVDF
Epoxy
30-40Å
2.0
1.5
1.0
0.5
0.0
Density (g/cm3)
PVDF
Epoxy
0
20
40
60
z(Å)
100
double
loop
Co-curing